*Supplement of*

# A 10 m vertical displacement on the Romanian Black Sea coast during modern history

Virgil Dragusin et al.

*Correspondence to*: Virgil Drăgușin (virgil.dragusin@iser.ro)

## 1. Historical development

The ancient city of Callatis was established in the 5th-4th century BCE as a colony of the Greek city of Heracleea Pontica and functioned as a maritime port while also having an important agricultural role. During the medieval period it was used as a harbor (when it is referred to as Pangalla) and saw a tumultuous evolution marked by Tatar invasions and wars between the Russian and Ottoman empires, usually resulting in the town being destroyed and reduced to a village. After the Romanian independence war, the region of Dobrogea became part of the Romanian Principalities in 1878. During the early 20th century, Mangalia became a hotspot for tourism and was developed into a city and important military harbor after the Second World War. Prior to the construction of the Mangalia Shipyard, a large swathe of sea bottom in front of the city was dredged down to the base rock, erasing the archaeological deposits.

The city's stadium and a park, the study area of the present work, were built in the 1950's, on an empty plot. On early 20th century maps, this area is partly occupied by a stand of trees surrounded by a stone wall (Fig. S1). On the same map, several small valleys appear to converge to the west of this depression and drain towards the sea along an intermittent creek that follows the southern edge of the study area. This creek was later transformed into a channel and was draining below the sea surface through a pipe that was still visible on satellite/aerial images in the 1960's.

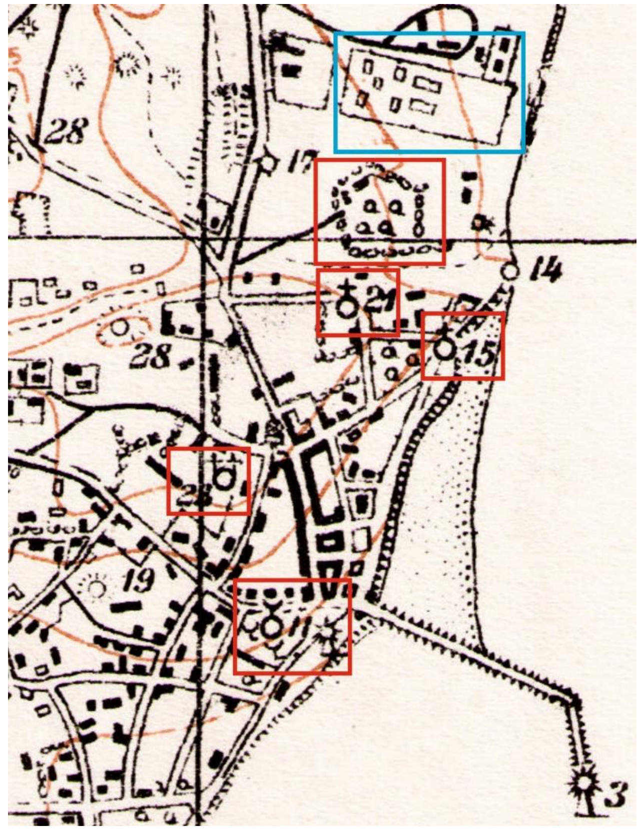


**Fig. S1 – Detail from the early 20th century map. The tree stand surrounded by the stone wall (red rectangle) and the houses belonging to the Principele Carol I Foundation (blue rectangle). Note that elevations are reported to an unknown datum. Numbers on the map depict: 11- Esmahan Sultan mosque and old lighthouse; 15 - the Greek church demolished in the 1960's; 21-old Romanian church; 28 – new Romanian church built in the 1920's. Image source: https://geo-spatial.org/vechi/download/planurile-directoare-de-tragere.**

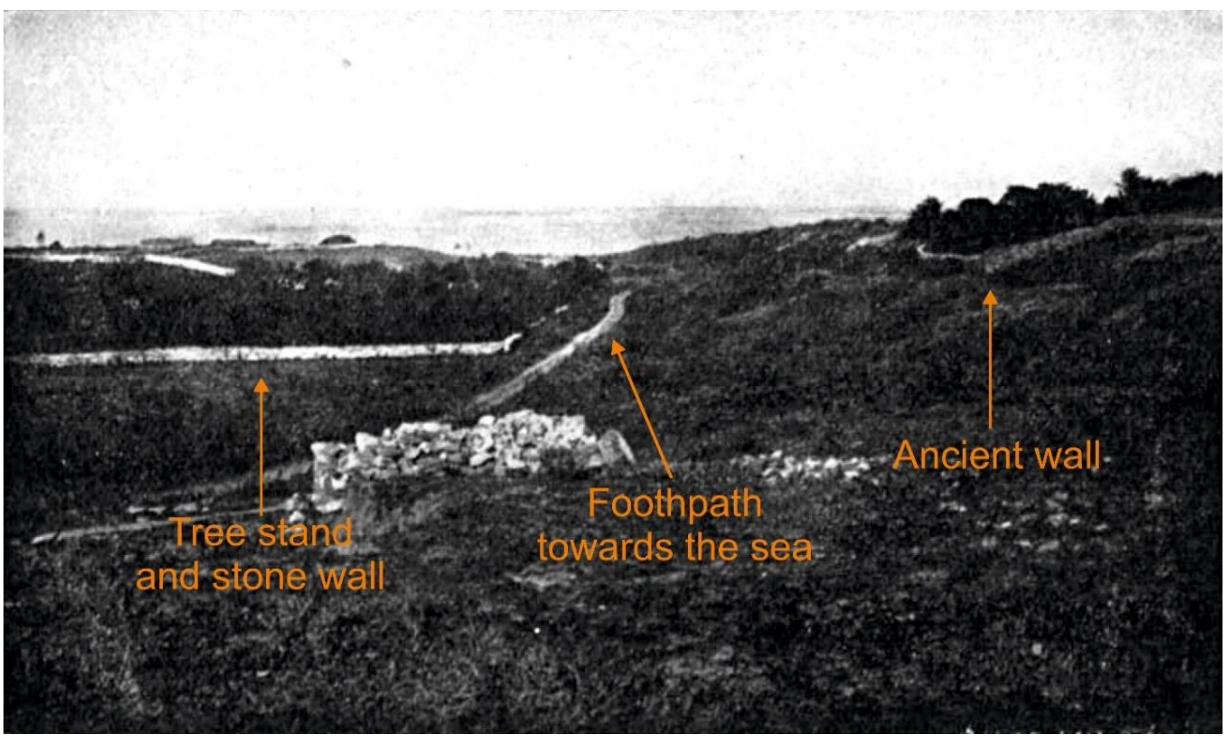


**Fig. S2. View (from the west) of the ancient wall on the right and the tree stand surrounded by a stone wall on the left, in 1926 (from Sauciuc-Săveanu, 1933). A footpath is visible along the intermittent creek.**

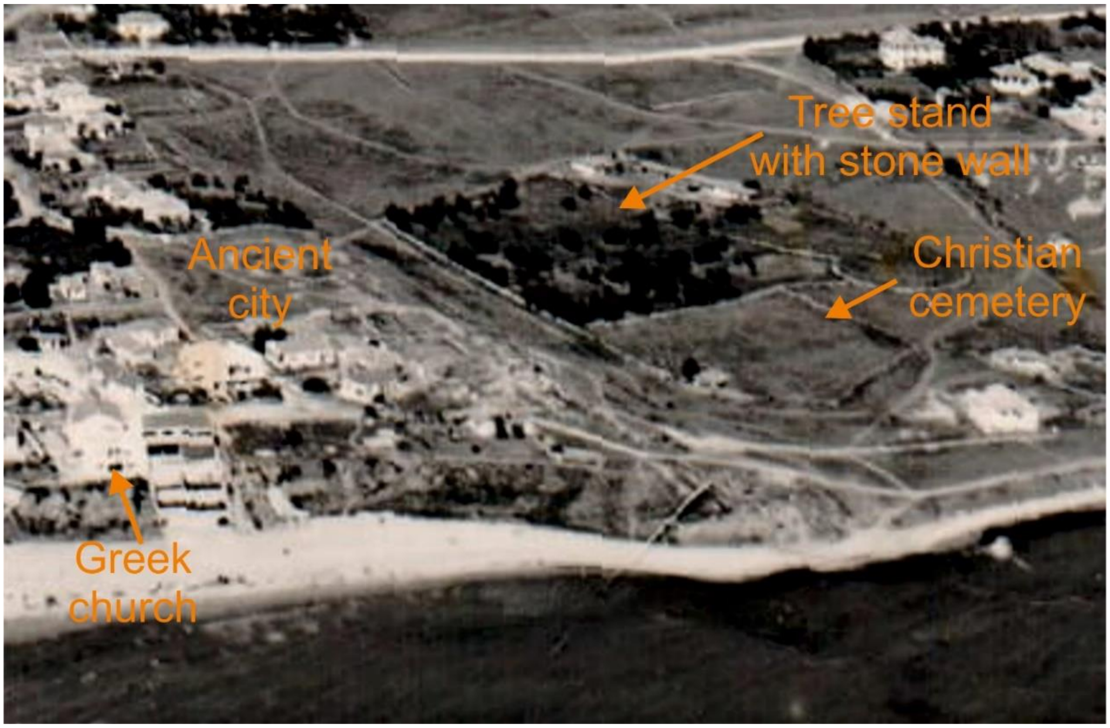


**Fig. S3. Aerial view of the northern part of Mangalia, taken from the east, during the 1930's.**

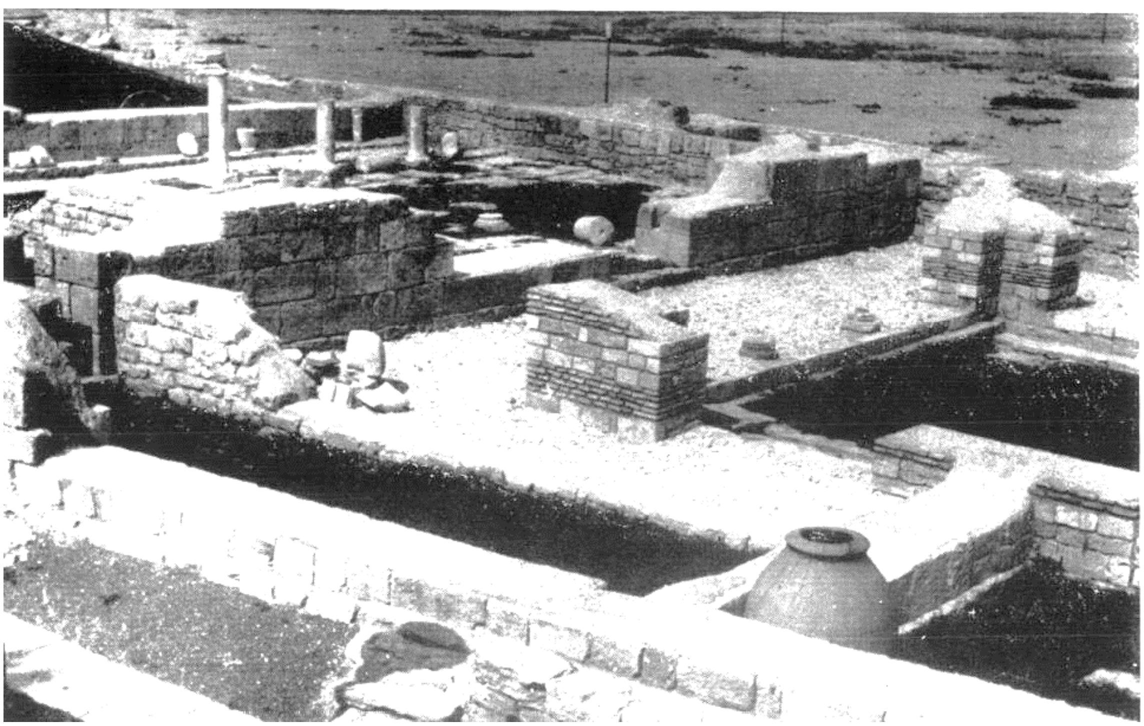

**Fig. S4. View from the ruins of the ancient city, towards the NW, with the sand surface covered in sparse vegetation in the background, probably taken during the early 1950's (from Preda, 1962).**

**Fig. S5. View from the ruins of the ancient city, towards the NW, with the new stadium and park, in the 1950-60's.**

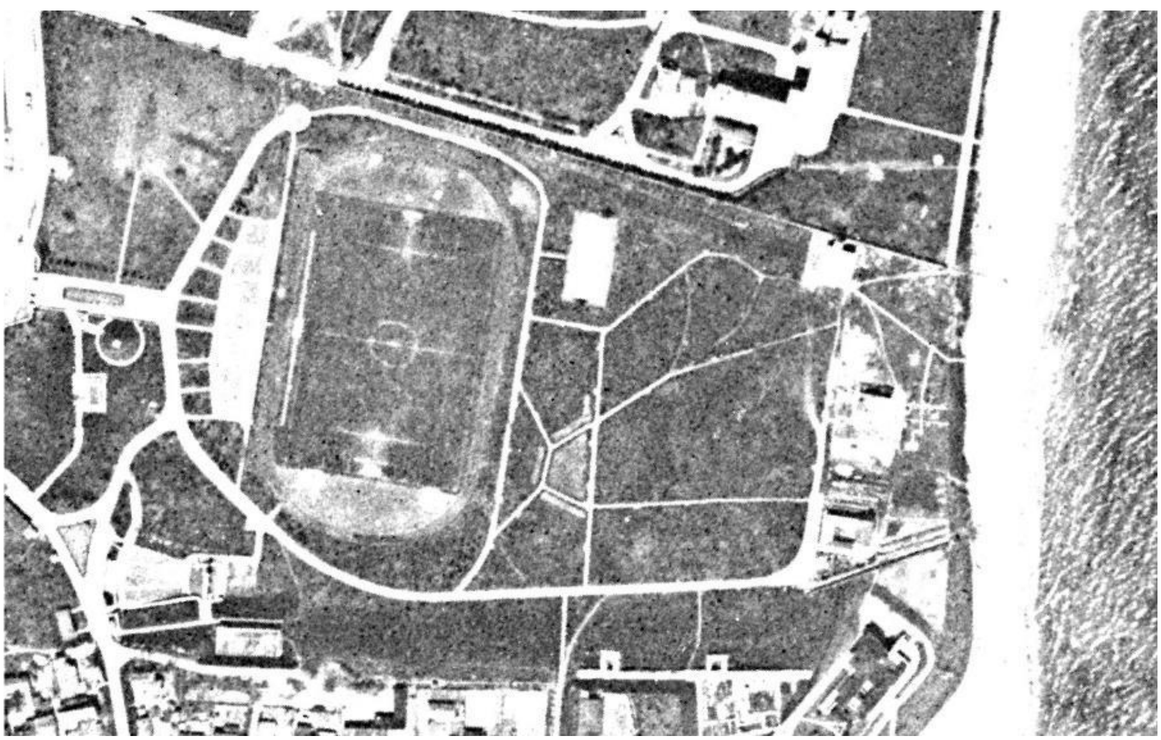

**Fig. S6. Satellite image showing the stadium and park. In the lower part of the image, the northern city wall with the two towers is visible. Image source: USGS (https://earthexplorer.usgs.gov/), entity ID DZB00402700026H018001. Image date: 1966**

## 2. Materials and methods

### 2.1. Structural framework

The structural model of Southern Dobrogea proposed by Popa et al. (2019) is based on 2D seismic survey conducted during 2013-2014 for shale gas potential over some 3500 $km^2$, combined with information from the logs of >200 boreholes with depths between 100 and 500 m and some even up to 1000 m.

The seismic survey grid, grouped in the three exploration perimeters, included a total of 800 km of linear distances distributed on 45 seismic profiles. The methodology was based on the correlation of small distance between channels and the depth of investigation. The generation of the seismic signal was performed using the Vibroseis technique (for 90% of generation points, 12 seconds of controlled vibration) and by controlled detonation of 1.5-5kg of explosive material at 10-15m in depth (for 10% of the points).

The primary data and the detailed interpretation methodology are confidential and can be obtained only upon request from the Romanian National Agency for Mineral Resources. The resulting configuration of the Valanginian (Lower Cretaceous) top surface was a secondary goal of the 2D seismic surveys, in the framework of a commercial contract between the University of Bucharest and Chevron Romania Exploration and Production S.R.L. and was intended to study the geometry of the aquifers overlapping the shale target zones. The schematic structure was published by Popa et al. (2019).

Some of the results of this regional seismic investigation pointed out that tectonic blocks are different in size and are separated by two fault systems oriented NNE-SSW and WNW-ESE. At the same time, the crystalline bedrock is steeply plunging westward (to the Danube River), leading to a significant increase of carbonate complex thickness (over 1000 m), trending upward towards the NE (north Constanta area) and plunging to the south and east (along the coastal area). Although Southern Dobrogea was thought to share with the Moesian Platform a relatively simple, platform-like evolution, the new seismic data shows that Southern Dobrogea area has a more complex geological structure.

### 2.2. Stratigraphy

Stratigraphy and sedimentology of the marine sediments that are the focus of this study were described from several profiles opened during construction works (TSC2, TSC3, TSC4, TSC11, TSC12, and TSC20), while at the other points we used a small diameter hand auger to investigate the sediments.

The marine sediments studied here are found at an altitude of ~10 m a.s.l. and were exposed during the construction of an engineering project, namely the renovation of the local stadium. In March 2022 a 1.7 m deep excavation was made with an area of ~400 $m^2$ and a perimeter of ~100 m. From the northern side of this excavation we describe the **TSC2** profile (Fig. S7, Fig. S8), with 1.7 m of open profile, extended by coring to 4.2 m, where it did not reach bedrock. In December 2022 another excavation was made, with a depth of 4.7 m (**TSC3**, Fig. S9) and a third excavation with a depth of 3.7 m was made in May 2023 (**TSC4**, Fig. S10). Other profiles, not depicted in figures, were:

**TSC 5** – excavation along the southern slope; slope deposits, mixture of soil and archaeological materials.

**TSC 9** – 0-90 cm: modern infill; 90-135 cm: sand of unknown origin, probably from construction works but could also be part of Unit 2; 135-220 cm: soil; 220 cm: hard surface.

**TSC 10** – 0-70 cm: soil with rock fragments; 70 cm: hard surface.

**TSC 15** – 0-50 cm: recent beach sand; 50-60 cm: reddish clay.

**TSC 16** – 0-150 cm: dry, silty soil; 150 cm: hard surface.

**TSC 17** – 0-50 cm: soil; 50 cm: hard surface.

**Table S1**. Geographic (WGS84) coordinates of profiles and cores

| Site | Longitude | Latitude | Type | Depth (m) |
|---|---|---|---|---|
| TSC 2 | 28.58528 | 43.81533 | excavation + core | 4.2 |
| TSC 3 | 28.58568 | 43.81523 | excavation | 4.7 |
| TSC 4 | 28.58565 | 43.81512 | excavation | 3.7 |
| TSC 5 | 28.58543 | 43.81501 | excavation | 1.5 |
| TSC 6 | 28.58586 | 43.81561 | core | 6.1 |
| TSC 7 | 28.58580 | 43.81628 | core | 4.3 |
| TSC 8 | 28.58614 | 43.81559 | core | 5.7 |
| TSC 9 | 28.58717 | 43.81503 | core | 2.2 |
| TSC 10 | 28.58676 | 43.81504 | core | 0.7 |
| TSC 11 | 28.58508 | 43.81598 | excavation | 1.2 |
| TSC 12 | 28.58478 | 43.81614 | excavation | 1.4 |
| TSC 13 | 28.58734 | 43.81560 | core | 3.4 |
| TSC 14 | 28.58780 | 43.81539 | core | 1.5 |
| TSC 15 | 28.58804 | 43.81574 | core | 0.6 |
| TSC 16 | 28.58758 | 43.81513 | core | 1.5 |
| TSC 17 | 28.58770 | 43.81647 | core | 0.5 |
| TSC 19 | 28.58764 | 43.81545 | core | 0.5 |
| TSC 20 | 28.58453 | 43.81508 | excavation | 3.0 |

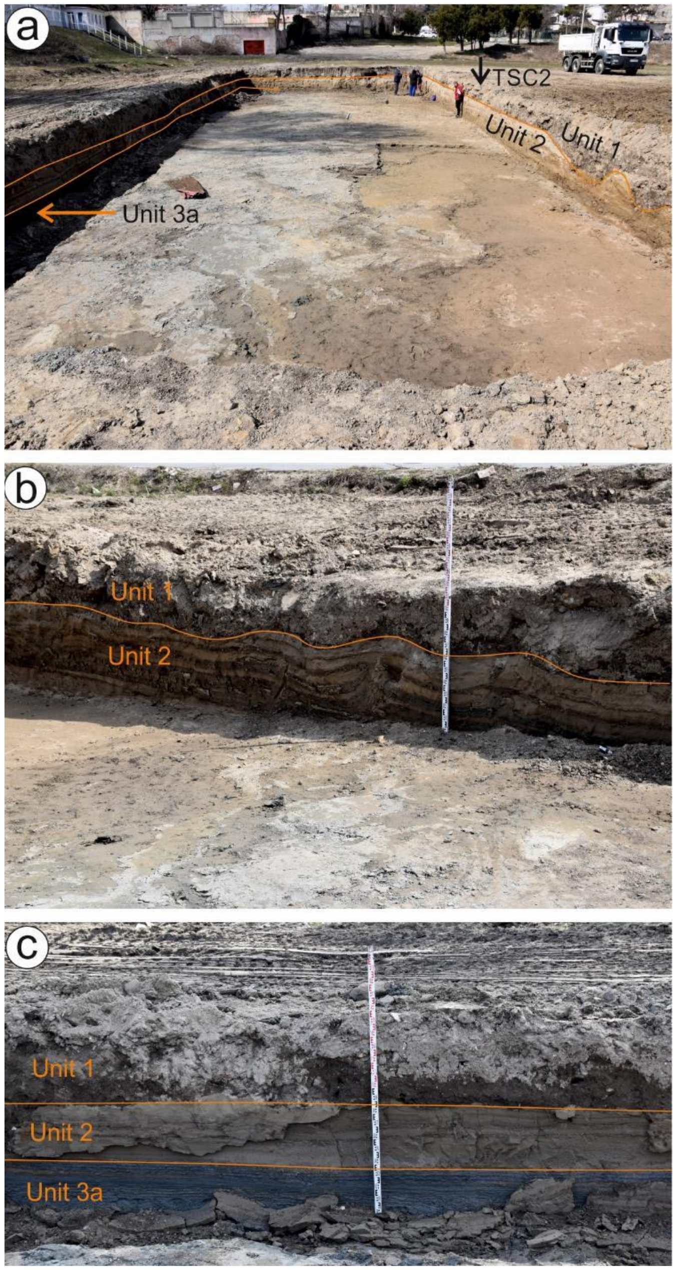


**Fig. S7 – a. Location of the TSC2 profile within the larger excavation (view from the east); b. eastern side of the excavation; c. southern side of the excavation.**

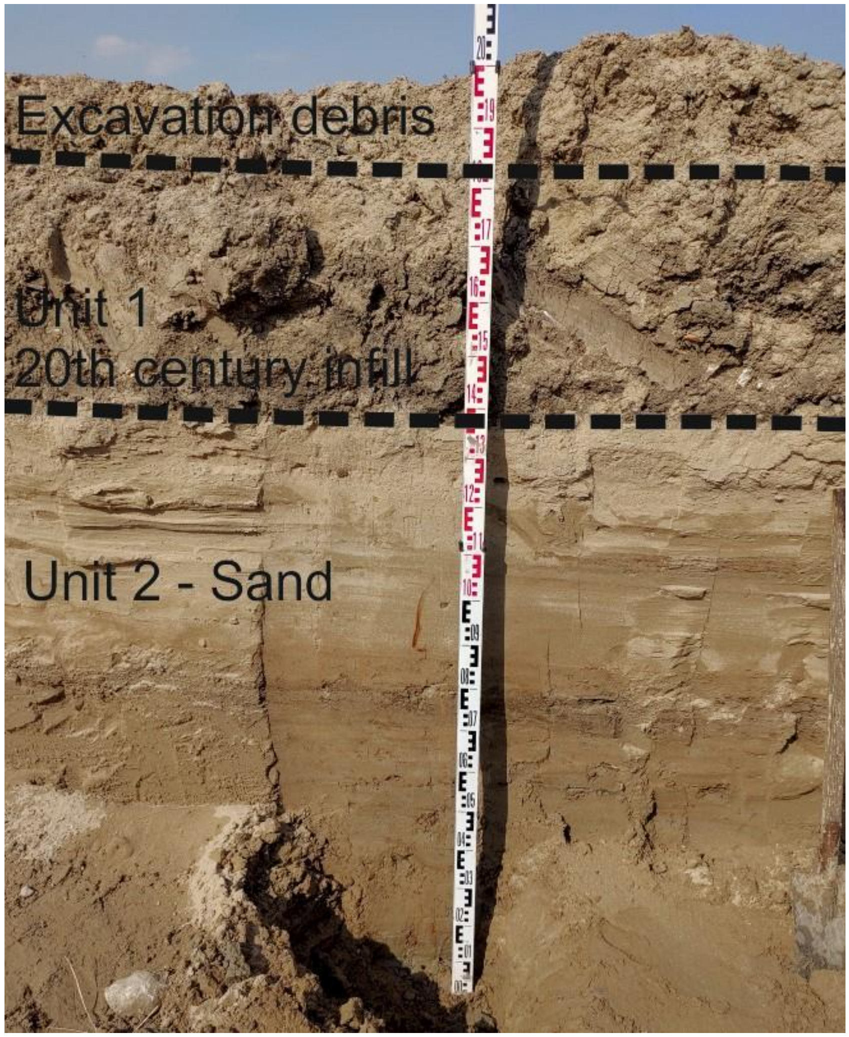


**Fig. S8 – Detail from the TSC2 profile**

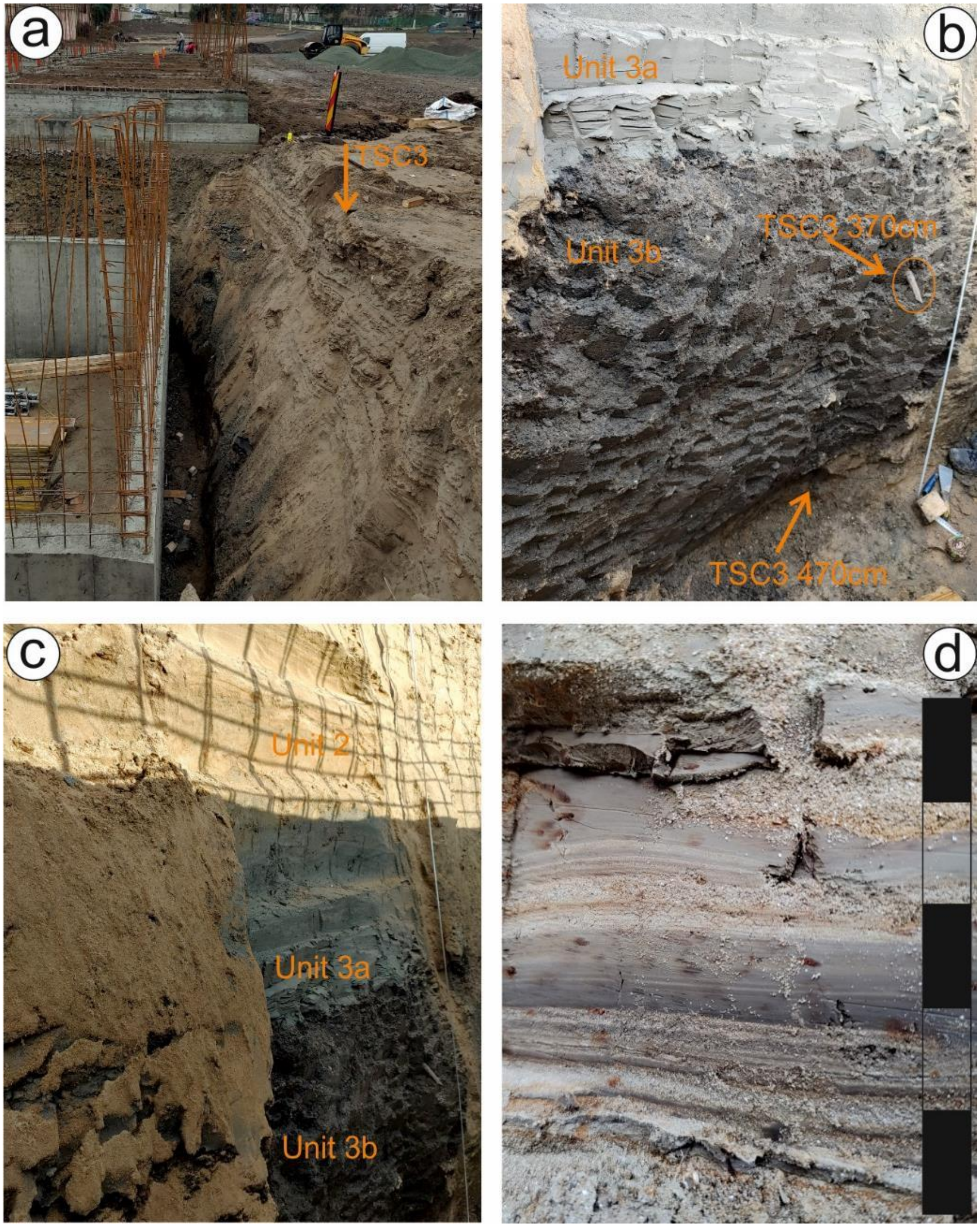


**Fig. S9 – a. Location of the TSC3 profile; b. lower part of the TSC3 profile with indications of the position of plant and bone samples used in radiocarbon dating; c. detail from the TSC3 profile;d. small detail from the top of Unit 3a, scale is 5 cm.**


**Fig. S10 – a. Excavation seen from the east; b. northern side of the excavation, during sampling from the TSC4 profile.**

**Fig. S11 – Charcoal-rich layers at the top of the sands in TSC4. The same layer yielded the large charcoal sample TSC 4-Carb-01 and bivalve samples TSC 4-Biv-01 and TSC 4-Biv-02. Scale is 100 mm.**

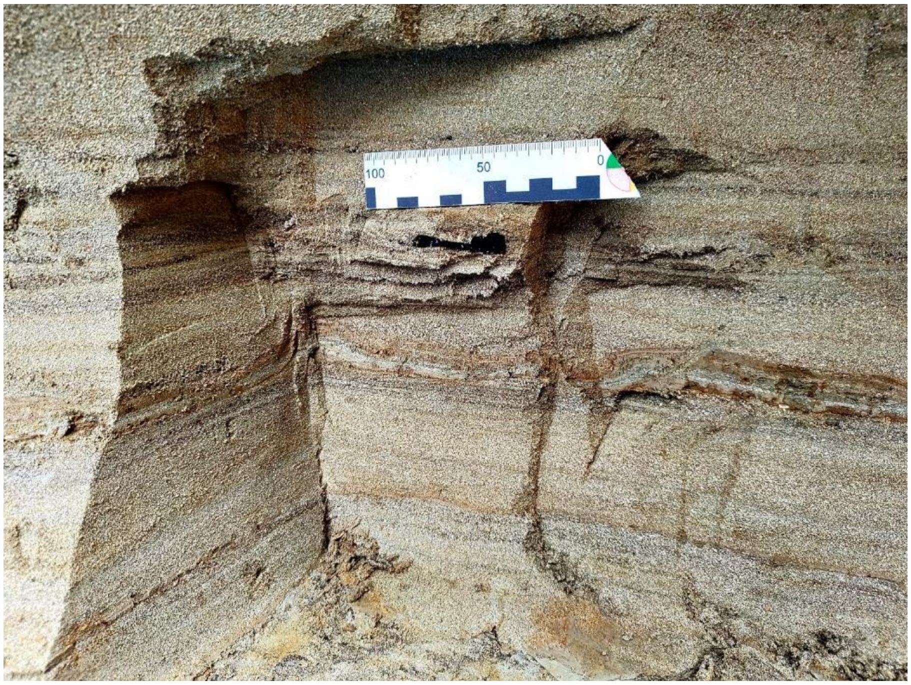


**Fig. S12 – Location of charcoal sample TSC 4-Carb-01. Scale is 100 mm.**

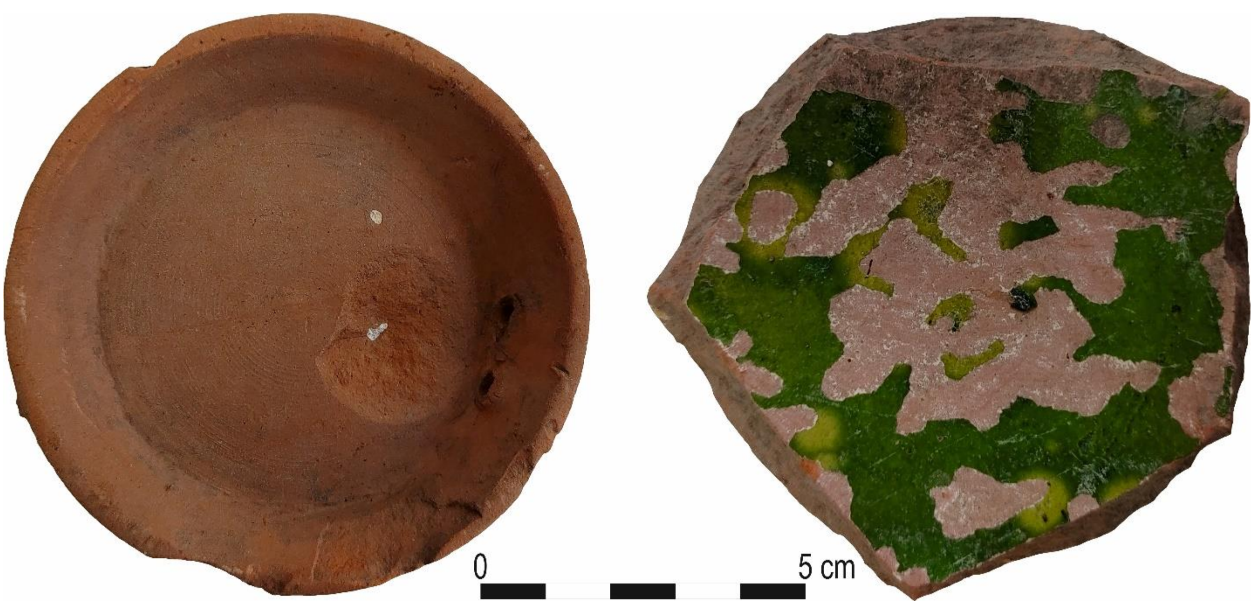


**Fig. S13 – Ottoman bowl fragment retrieved from Unit 3b in TSC 4, bottom view (left) and top view (right).**

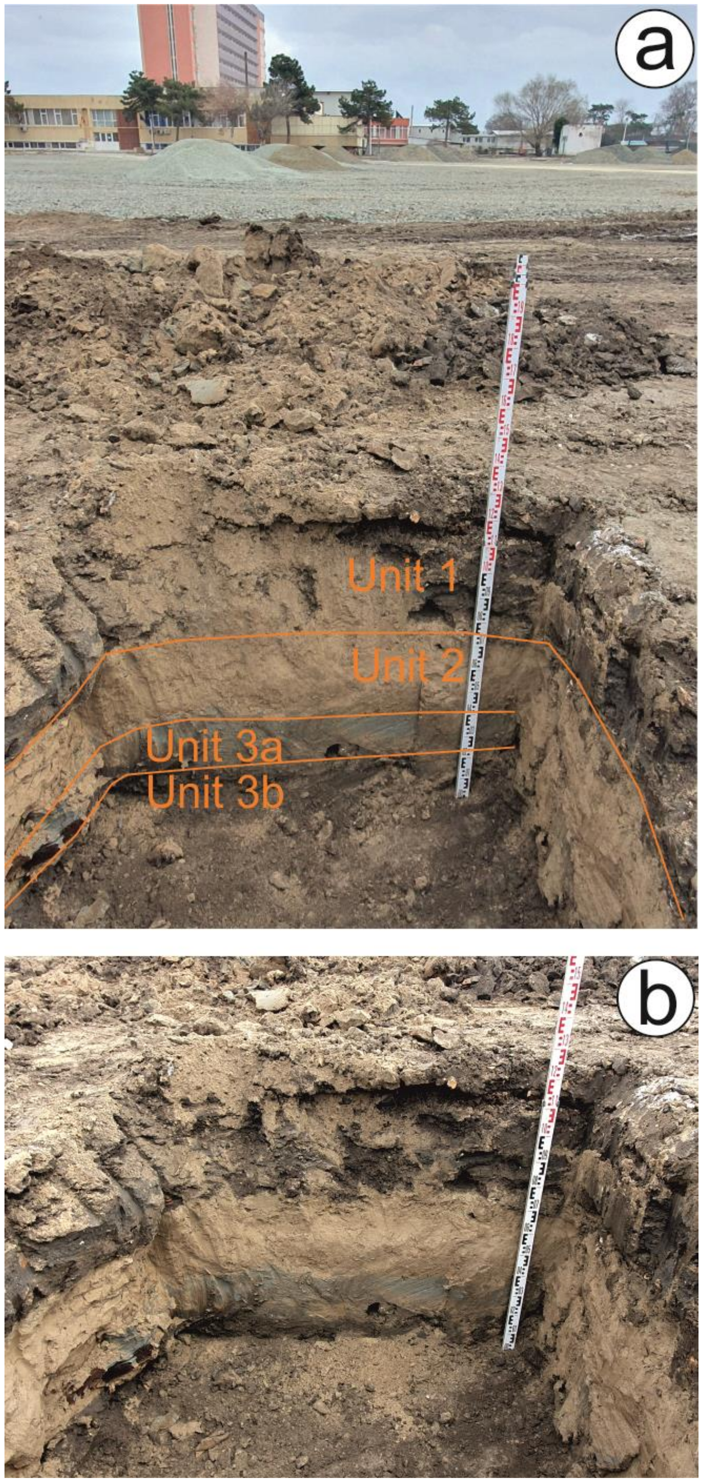


**Fig. S14 – Views from the west of the TSC11 profile**


130 **Fig. S15 – Views of the TSC12 profile, towards the south, with only anthropogenic infill visible**

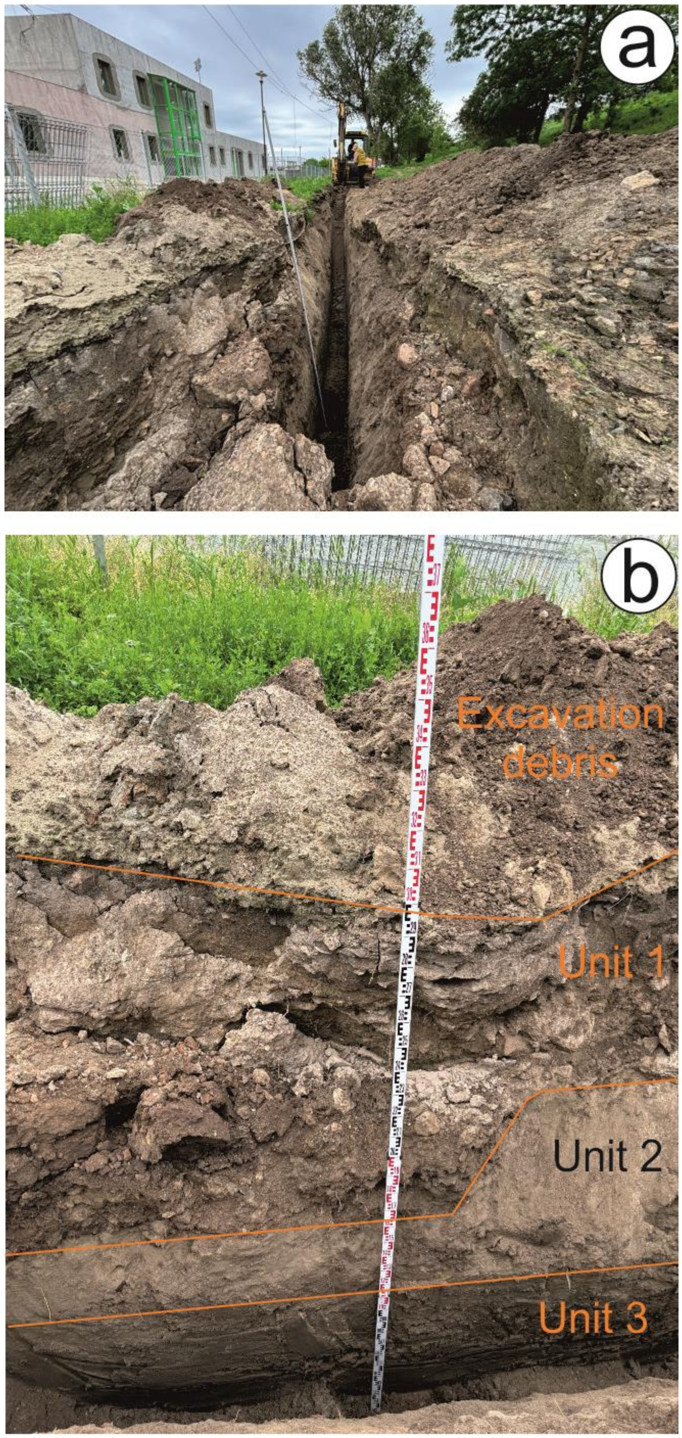


**Fig. S16 – Profile TSC20: a. view from the west; b. view from the south.**

135

**3. Results**

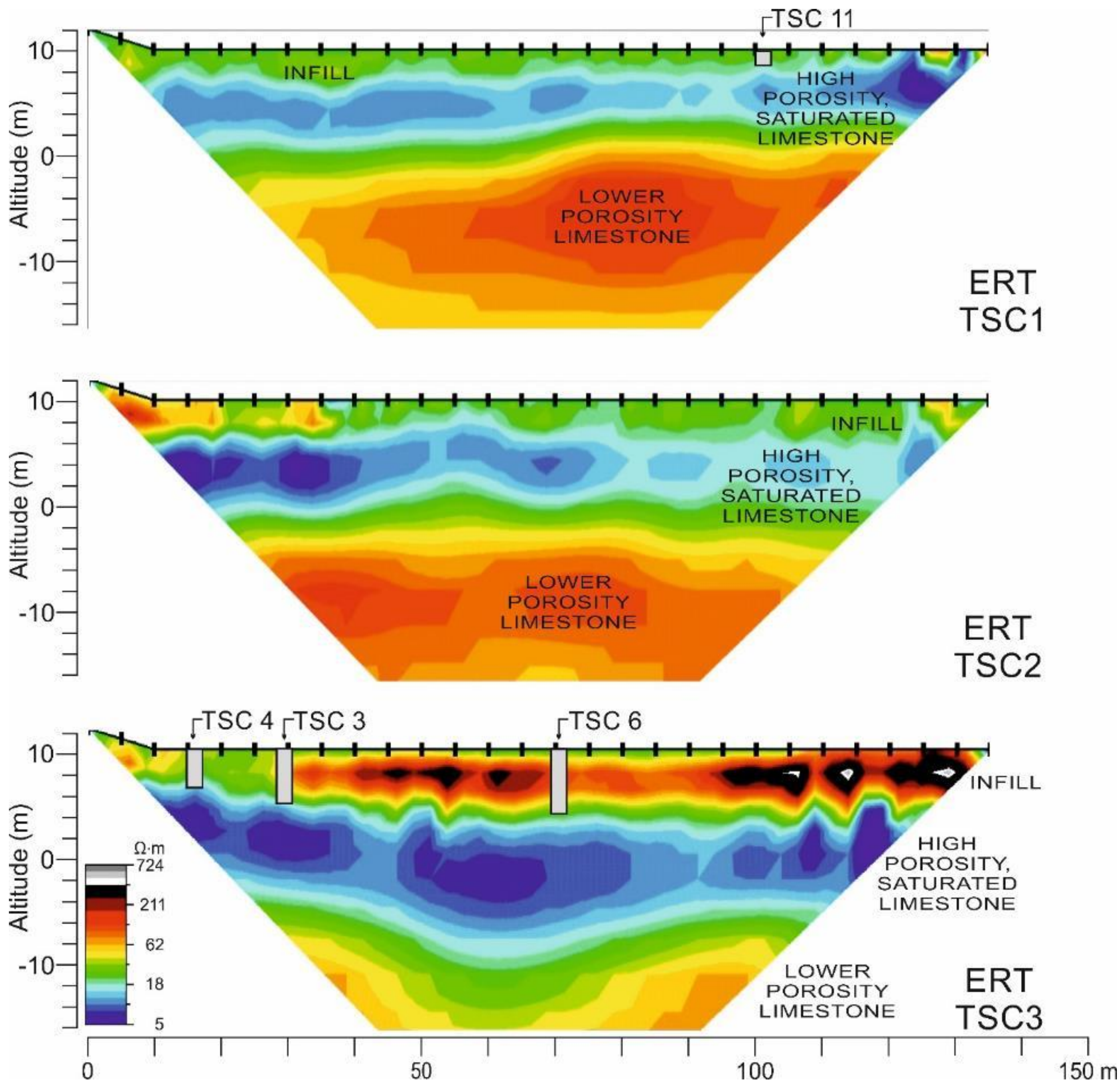


**Fig. S17 – ERT profiles. Grey bars represent profiles and cores, drawn at the same vertical scale as the ERT data.**


**Fig. S18 – Georadar profile locations. Base image: August 2022, Maxar/ESRI Map Viewer.**

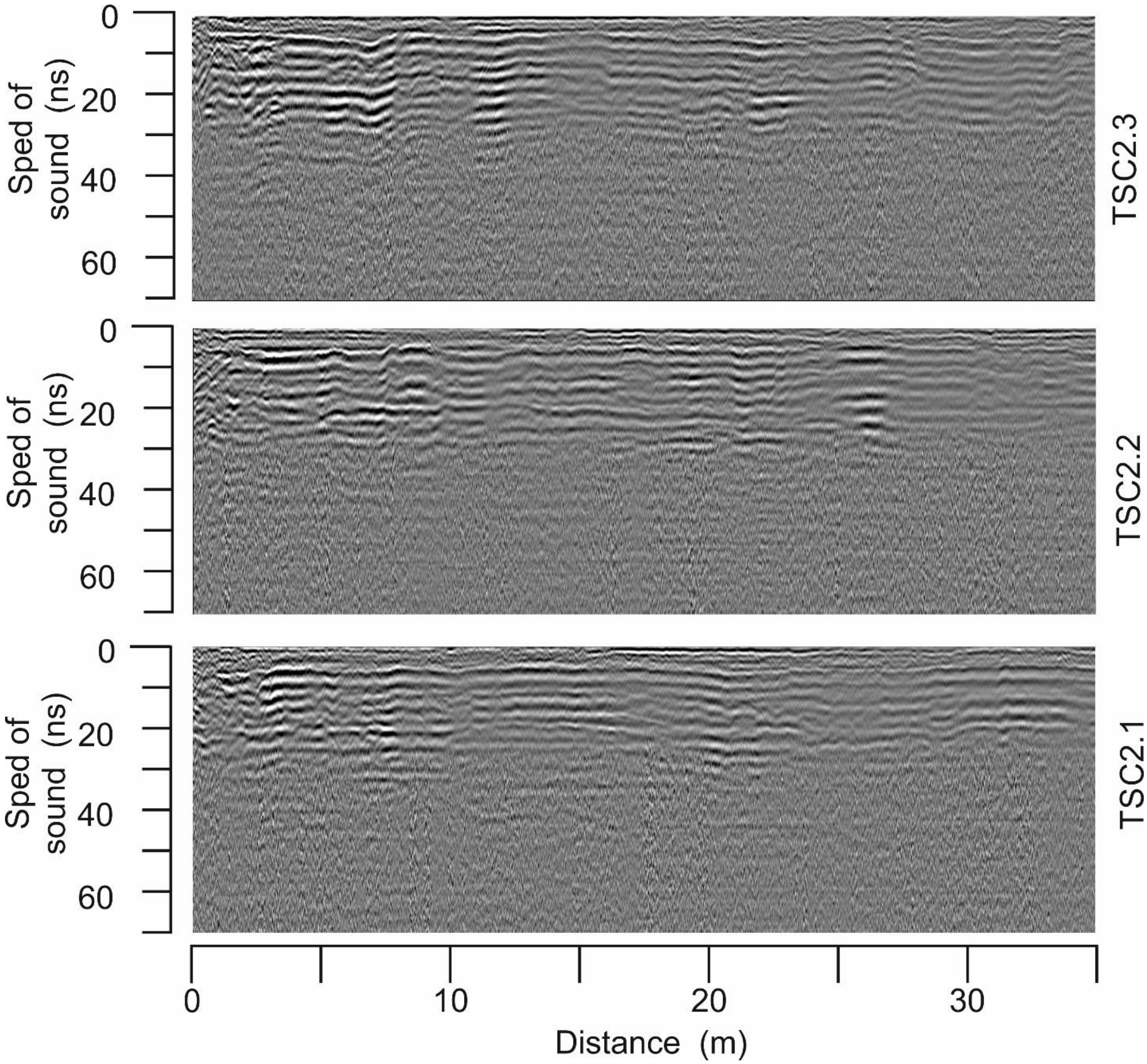


**Fig. S19 – Examples of GPR profiles.**

**Table S2**. Grain size, water content and electrical conductivity values. Water content was determined by drying at 50°C for 24 hours, while electrical conductivity (EC) was measured in a solution of sediment and ultrapure water in a 1:10 ratio.

| Sample ID | Depth (m) | Unit | Description | Clay (%) | Silt (%) | Sand (%) | Pebbles (%) | Water (%) | EC (µS/cm) |
|---|---|---|---|---|---|---|---|---|---|
| TSC 3-12 | 1.30 | 2 | clay/sandy silt | 33 | 47 | 20 | 0 | N/A | N/A |
| TSC 3-11 | 2.05 | | clayey sand/well graded sand | 10 | 24 | 66 | 0 | N/A | N/A |
| TSC 3-10 | 2.85 | | clayey sand/well graded sand | 6 | 14 | 80 | 0 | N/A | N/A |
| TSC 3-9 | 3.10 | 3a | sandy silty clay/silty sand | 13 | 34 | 53 | 0 | N/A | N/A |
| TSC 3-8 | 3.20 | | silty clay/silt | 36 | 62 | 2 | 0 | N/A | N/A |
| TSC 3-7 | 3.30 | | silty clay/silt | 37 | 62 | 1 | 0 | N/A | N/A |
| TSC 3-5 | 3.45 | 3b | silty clay/silt | 25 | 65 | 10 | 0 | N/A | N/A |
| TSC 3-4 | 3.70 | | silty clay/silt | 25 | 64 | 11 | 0 | N/A | N/A |
| TSC 3-3 | 4.00 | | silty clay/silt | 26 | 64 | 10 | 0 | N/A | N/A |
| TSC 3-2 | 4.65 | | silty clay/silt | 26 | 61 | 13 | 0 | N/A | N/A |
| TSC 3-1 | 4.78 | 3c | silty clay/silt | 38 | 58 | 4 | 0 | N/A | N/A |
| TSC 4-1 | 0.6-0.7 | 2 | sand/uniformly graded sand | 0 | 3 | 97 | 0 | 7 | 57 |
| TSC 4-2 | 1.80-1.90 | 3a | sand/uniformly graded sand | 0 | 11 | 89 | 0 | 18 | 283 |
| TSC 4-3 | 2.00-2.10 | | clayey sand/well graded sand | 9 | 17 | 74 | 0 | 24 | 760 |
| TSC 4-4 | 2.30-2.40 | | clay/silt | 40 | 59 | 1 | 0 | 31 | 1730 |
| TSC 4-5 | 2.70 | 3b | silty clay/silt | 22 | 65 | 13 | 0 | 24 | 778 |
| TSC 4-6 | 2.90-2.95 | 3c | silty clay/silt | 23 | 63 | 14 | 0 | 21 | 600 |
| TSC 4-7 | 2.95-3.00 | | sandy silty clay/silt | 21 | 55 | 20 | 4 | 21 | 609 |
| TSC 4-8 | 3.00-3.05 | | silty clay/sandy silt | 22 | 61 | 17 | 0 | 21 | 575 |
| TSC 4-9 | 3.05-3.10 | | silty clay/sandy silt | 23 | 60 | 17 | 0 | 20 | 580 |

**Table S3**. Mineralogical composition

| Sample ID | Depth (m) | Unit | Quartz (%) | Calcite (%) | Plagiocalase (%) | Muscovite (%) | Chlorite (%) | Aragonite (%) | Dolomite (%) |
|---|---|---|---|---|---|---|---|---|---|
| TSC 4-1 | 0.6-0.7 | 2 | 31 | 25 | 0 | 9 | 0 | 36 | 0 |
| TSC 4-2 | 1.80-1.90 | 3a | 50 | 9 | 5 | 19 | 0 | 10 | 7 |
| TSC 4-3 | 2.00-2.10 | | 84 | 4 | 0 | 12 | 0 | 0 | 0 |
| TSC 4-4 | 2.30-2.40 | | 51 | 15 | 10 | 20 | 4 | 0 | 0 |
| TSC 4-5 | 2.70 | 3b | 73 | 11 | 7 | 5 | 0 | 0 | 4 |
| TSC 4-6 | 2.90-2.95 | 3c | 61 | 13 | 8 | 19 | 0 | 0 | 0 |
| TSC 4-7 | 2.95-3.00 | | 70 | 11 | 12 | 7 | 0 | 0 | 0 |
| TSC 4-8 | 3.00-3.05 | | 82 | 5 | 8 | 5 | 0 | 0 | 0 |
| TSC 4-9 | 3.05-3.10 | | 71 | 14 | 8 | 7 | 0 | 0 | 0 |
| TSC 6 510 | 5.10 | 4a | 40 | 34 | 0 | 26 | 0 | 0 | 0 |
| TSC 6 530 | 5.30 | | 58 | 19 | 0 | 12 | 11 | 0 | 0 |
| TSC 6 585 | 5.85 | 4b | 42 | 16 | 0 | 31 | 11 | 0 | 0 |


**Fig. S20 – Ostracod and foraminifer fauna, retrieved by sieving using the method described in Neagu and Dragomir (1982). 1, 2. *Cyprideis* littoralis; 3. *Loxoconcha* sp.; 4. *Leptocythere* sp.; 5, 6. *Ammonia beccarii*; 7, 8. *Elphidium* sp.; 9-11. *Quinqueloculina* sp.**

**Table S4.** List of non-pollen palynomorphs identified in the archaeological layer (Unit 3b), identified following Shumilovskikh et al. (2021), and using the NPP database http://non-pollen-palynomorphs.uni-goettingen.de.

| **Palynomorphs** | **Taxonomical group** |
|---|---|
| *Botryococcus* | Green algae |
| *Arnium*-type | Fungi |
| *Chaetomium* | Fungi |
| *Coniochaeta ligniaria* | Fungi |
| *Glomus*-type | Fungi |
| *Podospora* group<br>*Mediaverrunites* | Fungi<br>Fungi |
| *Sordaria*- type | Fungi |
| *Puccinia* | Fungi |
| *Sporormiella*-type | Fungi |
| *Thecaphora* | Fungi |

**Table S5**. Result of radiocarbon dating

| **Sample Code** | **ROAMS code** | **Type** | **C/N** | **Atomic C/N** | **$^{14}$C age** | **error** |
|---|---|---|---|---|---|---|
| TSC 3 470 cm | 5430.5 | plant | 13.1 | 15.3 | 133 | 21 |
| TSC 3 370 cm | 5426.5 | bone | 3.0 | 3.5 | 239 | 23 |
| TSC 4-Os-01 | 5607.1 | bone | 2.7 | 3.2 | 497 | 40 |
| TSC 3-2 465 cm | 5431.5 | sediment | 13.3 | 15.6 | 2435 | 24 |
| TSC 3-6 335 cm | 5432.5 | sediment | 10.6 | 12.4 | 1114 | 25 |
| TSC 4-Biv-01 | 5609.1 | shell | N/A | N/A | 1066 | 33 |
| TSC 4-Biv-02 | 5610.1 | shell | N/A | N/A | 1018 | 34 |
| TSC 4-Carb-01 | 5606.1 | charcoal | 149.7 | 174.5 | 2971 | 64 |

**Table S6**. Isotopic values of *Cerastoderma edule* (TSC 4-Biv-01) and *Abra alba* (TSC 4-Biv-02) specimens.

| Sample ID | Distance from umbo (mm) | $\delta^{13}C$ (‰ vs VPDB) | $\delta^{18}O$(‰ vs VPDB) |
|---|---|---|---|
| TSC 4-Biv-01-1 | 4.2 | 0.03 | -2.6 |
| TSC 4-Biv-01-2 | 7.5 | -0.04 | -2.36 |
| TSC 4-Biv-01-3 | 10.6 | -1.91 | -5.8 |
| TSC 4-Biv-01-4 | 16.3 | -1.56 | -5.77 |
| TSC 4-Biv-01-5 | 21.1 | -0.76 | -3.92 |
| TSC 4-Biv-02-1 | - | -1.58 | -3.63 |

**References**


Popa, I., Mocuța, M., and Iurkiewicz, A.: A new regional conceptual model on the hydrogeology of Southern Dobrogea based on seismic surveys and hydro-geological data revisiting, in: Proceedings of 4th Conference of the IAH CEG, edited by: Stevanovic, Z., Zivanovic, V., and Milanovic P., International Association of Hydrogeologists (IAH) National Chapter (NC) of Serbia, 47–49, 2019.

Preda, C., Popescu, E., and Diaconu, P.: Săpăturile arheologice de la Mangalia (Callatis), Materiale şi cercetări arheologice, 8, 439-455, doi:10.3406/mcarh.1962.1307, 1962.

Sauciuc-Săveanu, T.: Callatis. III-e rapport préliminaire. Fouilles et recherches de 1926, Dacia, 3-4, 411-434, 1933.

Shumilovskikh, L. S., O'Keefe, J. M. K., and Marret, F.: An overview of the taxonomic groups of NPPs, in: Applications of Non-Pollen Palynomorphs from Palaeoenvironmental reconstructions to Biostratigraphy, adited by: Marret, F., O’Keefe, J., Osterloff, P., Pound, M., Shumilovskikh, L. S., Geological Society, London, Special Publications, 511, 13-61, doi:10.1144/SP511-2020-65, 2021.